Reviewers' Comments to Authors:

Reviewer #3 :

General Comments:

In this paper, the authors applied the Constituent-oriented Age and Residence Time Theory to the high-resolution ocean reanalysis GLORYS12 to study the ocean bottom-water return over the centennial timescale. They found and confirmed the dominant role of the Southern Ocean. The question addressed is clearly important in oceanography, and the authors conducted extensive analyses. As a colleague, I appreciate their efforts. That said, the current version of this manuscript has a few major issues that make it hard to follow and evaluate. I recommend a **major revision** before another round of review.

Response: We sincerely thank the reviewer for the thoughtful evaluation of our manuscript and for identifying several important issues concerning data robustness, methodological clarity, figure interpretation, and overall presentation. Following these comments, we have substantially improved the description and organization of the Methods, strengthened the assessment of the underlying reanalysis, and revised the figures and related text for greater clarity and consistency. We believe these changes have made the manuscript much easier to follow and evaluate.

My major comments are as follows:

Major Comments

1. The entire study is based on a single high-resolution ocean reanalysis. How reliable is that dataset? Are the conclusions drawn from analyses of that particular product robust? This should at least be discussed in the paper.

Response: Thank you for this important comment. We agree that the reliability of GLORYS12 and the extent to which the diagnosed patterns may depend on a single reanalysis should be discussed explicitly. We have therefore strengthened the description of GLORYS12 in the Methods and added several complementary checks to evaluate the aspects of the dataset most relevant to the present bottom-water analysis. These include a direct quality-control assessment of the three-dimensional neutral-density field, an independent comparison with the observationally based World Ocean Atlas 2023 (WOA23) climatology, and a quantitative regional decomposition of upward bottom-water transport. We have also expanded the Discussion to distinguish the robustness of the broad basin-scale conclusions from product-dependent uncertainty in more regional and quantitative features.

GLORYS12 is a data-assimilative global ocean reanalysis rather than a freely evolving model simulation. It combines a 1/12° eddy-rich ocean configuration with observational constraints from satellite altimetry, sea-surface temperature and sea-ice observations, and in situ temperature and salinity profiles. Previous regional and global assessments have demonstrated its ability to reproduce major circulation and hydrographic structures relevant to the present analysis (Artana et al., 2021; Du Pontavice et al., 2023; Jean-Michel et al., 2021; Lellouche et al., 2018; Verezemskaya et al., 2021).

To make this basis clearer, we expanded the opening description of GLORYS12 in Sect. 2.1. The revised text now reads:

> *"We use the GLORYS12 global ocean reanalysis from the Copernicus Marine Environment Monitoring Service (CMEMS) to diagnose bottom-water return pathways and timescales. GLORYS12 is a global high-resolution physical reanalysis with a nominal horizontal resolution of* $1/12°$*, 50 vertical levels, and coverage from 1993 to the present (Jean-Michel et al., 2021; Lellouche et al., 2018). The reanalysis assimilates multiple observational constraints, including satellite altimetry, sea-surface temperature and sea-ice observations, and in situ temperature and salinity profiles, using a reduced-order Kalman-filter framework; a three-dimensional variational procedure is additionally used to reduce slowly evolving large-scale temperature and salinity biases (Jean-Michel et al., 2021; Lellouche et al., 2018). Previous regional and global assessments have shown that GLORYS12 reproduces key large-scale circulation and hydrographic structures relevant to the present analysis (Artana et al., 2021; Du Pontavice et al., 2023; Verezemskaya et al., 2021)."*

Beyond these previous evaluations, we performed a direct quality-control assessment of the three-dimensional neutral-density field because the density structure provides the basis for the principal diapycnal diagnostics. The assessment shows that local neutral-density inversions are extremely rare and that the $\gamma^n = 28.1\ \mathrm{kg\,m^{-3}}$ surface used for the principal diapycnal-velocity analysis is effectively single-valued. To document this assessment transparently, we added a new Supplementary Text S1.

Supplementary Text S1 now reads:

> *"We assessed the geometry of the neutral-density field used for the isopycnal diagnostics by examining the original three-dimensional GLORYS12* γ^n *field before zonal averaging. Vertical model levels were examined sequentially from shallow to deep. For each pair of adjacent valid levels, an inversion was identified when the neutral density at the deeper level was lower than that at the immediately overlying shallower level, i.e.,* $\gamma^n_{deeper} - \gamma^n_{shallower} < 0$*. No additional numerical tolerance was imposed; any negative adjacent-level difference was counted as an inversion. The same three-dimensional neutral-density field is used for the cross-density diagnostics described in Sect. 2.3 of the main text. Among 218,683,701 valid adjacent vertical interfaces, 25,381 neutral-density inversions were identified, accounting for 0.0116% of the total. Of the 5,162,577 valid water-column profiles, 0.4858% contained at least one inversion. Among*

the affected profiles, 98.98% contained a single inverted interface, and 88.55% of all inversions occurred at the uppermost valid interface. Within the abyssal density range $\gamma^n = 28.1\text{–}28.2\ kg\ m^{-3}$*, 14 inversions were identified, corresponding to 0.0552% of the 25,381 inversions across the full density range.*

We also examined the vertical uniqueness of the $\gamma^n = 28.1\ kg\ m^{-3}$ *surface used in the principal diapycnal-velocity analysis. Among the 3,794,293 water-column profiles in which this density surface is present, 3,794,289 contain exactly one vertical crossing and four contain multiple crossings. The* $\gamma^n = 28.1\ kg\ m^{-3}$ *surface therefore has a single vertical intersection in all but four of the profiles in which it occurs. Its spatial depth distribution is shown in Fig. S4b. These checks characterize the vertical density geometry and the uniqueness of the surface intersections used in the cross-density diagnostics."*

We also compared the deep neutral-density structure with the observationally based WOA23 climatology. The zonal-mean sections reproduce broad basin-scale stratification, while the $\gamma^n = 28.2$ kg m^{-3} contour extends farther north in GLORYS12 than in WOA23 in the Atlantic, Pacific, and Indian Oceans. Supplementary Text S1 and Figs. S8–S9 document this agreement in the broad structure together with differences in dense-water extent.

The WOA23 zonal-mean comparison is shown in Supplementary Fig. S8 below:

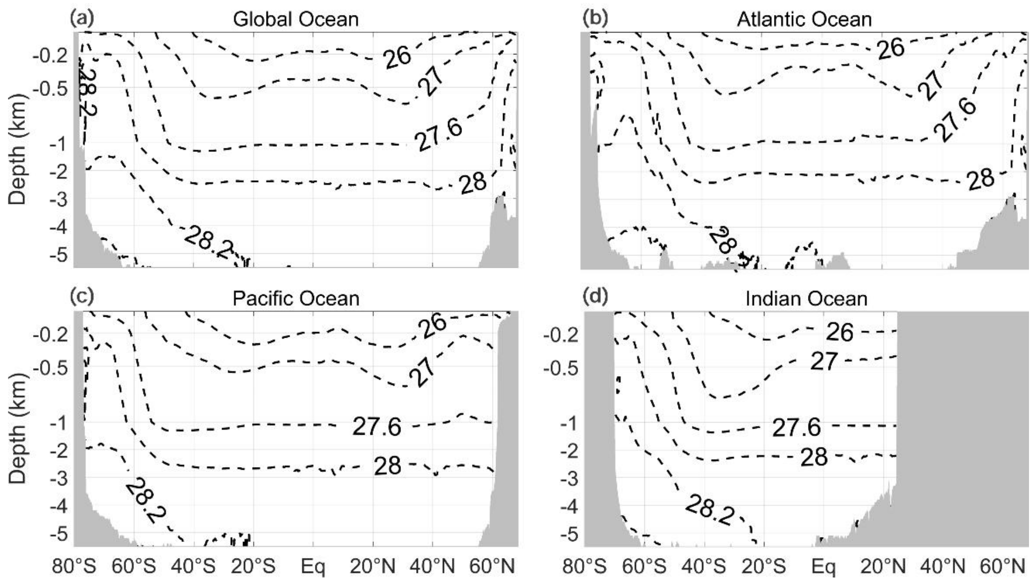

"Figure S8. Zonal-mean neutral density (γ^n, kg m^{-3}) calculated from the World Ocean Atlas 2023 (WOA23) climatology in depth–latitude coordinates for the (a) global ocean, (b) Atlantic Ocean, (c) Pacific Ocean, and (d) Indian Ocean. The contours provide a hydrographic comparison with the GLORYS12 zonal-mean sections in Fig. S3."

The bottom-density comparison is shown in Supplementary Fig. S9 below:

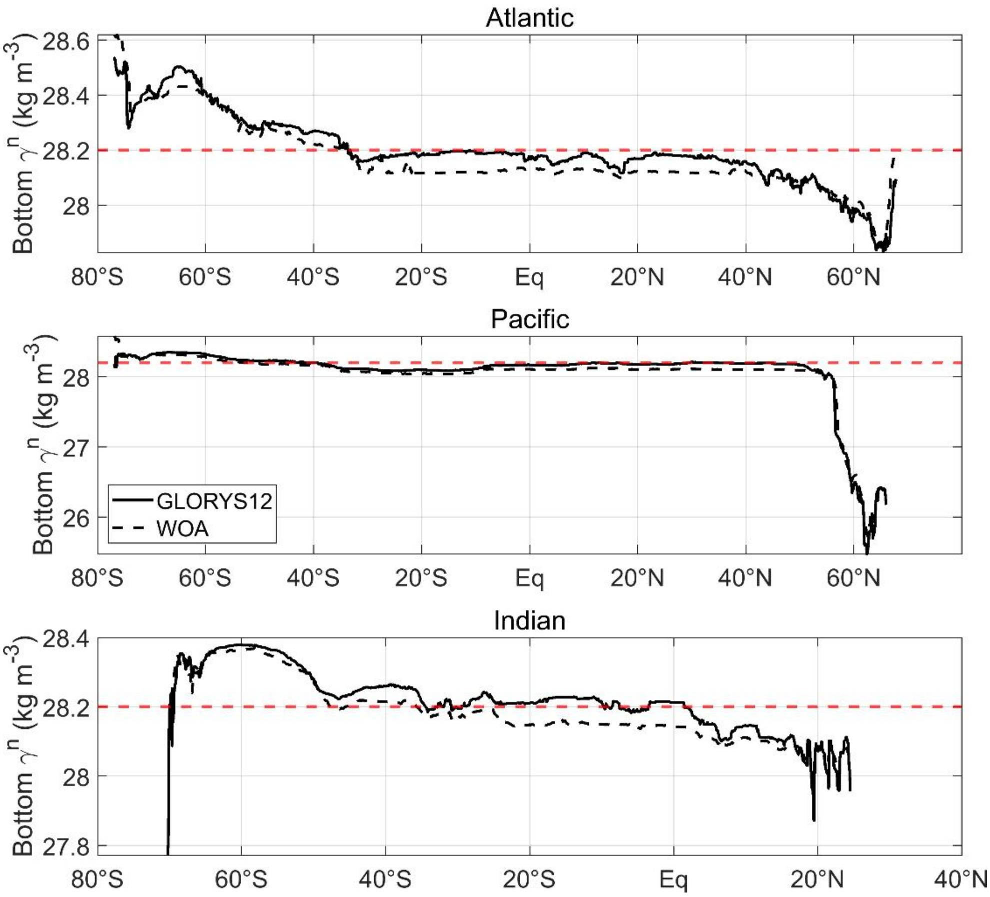

"Figure S9. Zonal-mean bottom neutral density (γ^n , $kg\,m^{-3}$) from GLORYS12 (solid black lines) and the World Ocean Atlas 2023 (WOA23) climatology (dashed black lines) in the Atlantic (top), Pacific (middle), and Indian Ocean (bottom). Red dashed lines mark $\gamma^n = 28.2\ kg\,m^{-3}$. The vertical scales differ among panels."

The added Supplementary Text S1 now reads:

"An additional hydrographic comparison uses neutral density calculated from the World Ocean Atlas 2023 (WOA23) climatology. The zonal-mean sections show broadly similar basin-scale stratification in GLORYS12 and WOA23 (Figs. S3 and S8). However, the $\gamma^n = 28.2\ kg\,m^{-3}$ contour extends farther north in the GLORYS12 sections than in the WOA23 sections of the Atlantic, Pacific, and Indian Oceans. The bottom-density comparison (Fig. S9) also shows differences near this density label. Differences in bottom density near a specified label can change whether that surface occurs in a water column and where it meets the lower boundary. The contours in Figs. S3 and S8 are constructed from zonal-mean density fields and do not trace the connectivity of individual three-dimensional surfaces. The mapped GLORYS12 surface in Fig. S4b is instead obtained from individual profiles. The profile checks and hydrographic comparison therefore address distinct aspects of the

diagnostics: the former quantify inversions and surface intersections, while the latter identifies differences in the represented dense-water extent."

The regional transport analysis provides an additional diagnostic within GLORYS12. We integrated upward concentration-weighted diapycnal transport over the Southern Ocean south of 40°S and the Atlantic, Pacific, and Indian Oceans north of 40°S. The Southern Ocean provides the largest individual regional contribution over most of the deep and abyssal density range, reaching about 5 Sv near $\gamma^n \approx 28.2$ kg m^{-3}. The separate regional curves peak at approximately 4.0 Sv in the Pacific, 2.3 Sv in the Atlantic, and 1.3 Sv in the Indian Ocean. Published transport estimates provide context, with the differences in source definitions, boundaries, and transport measures described in the Introduction.

To make this regional comparison explicit, we added Supplementary Fig. S5. The new figure and its caption are:

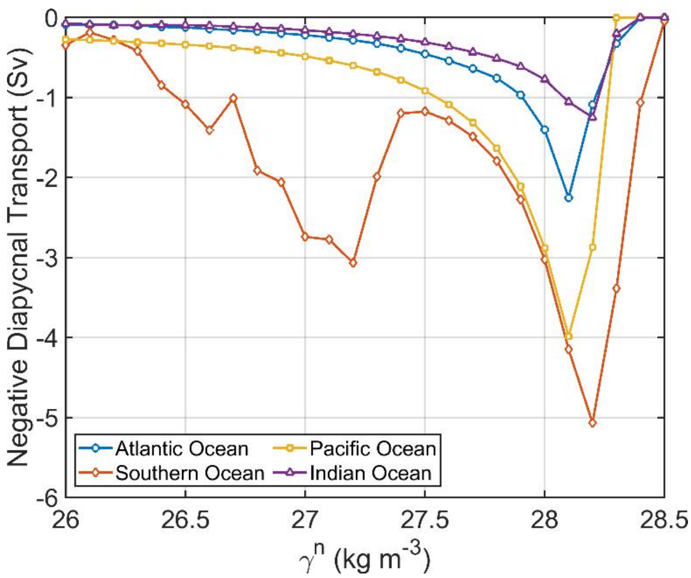

"Figure S5. Regional upward concentration-weighted diapycnal transport (Sv) across neutral-density surfaces spaced at intervals of $0.1\ kg\,m^{-3}$ *for the Southern Ocean south of 40° S and the Atlantic, Pacific, and Indian Oceans north of 40° S. Negative values denote transport toward lighter density classes, following the sign convention in Sect. 2.4 of the main text. Each curve shows the density dependence of one regional contribution. Contributions across a common surface are compared at the same neutral density."*

Following this additional analysis, the corresponding text added to the revised manuscript reads:

"To quantify the regional distribution of upward bottom-water transport, we further integrated the upward concentration-weighted diapycnal flux separately over the Southern Ocean south of 40°S and over the Atlantic, Pacific, and Indian Oceans north of 40°S (Supplementary Fig. S5). The

Southern Ocean exhibits the largest individual regional contribution to upward concentration-weighted transport over most of the abyssal-to-deep density range, with a peak magnitude of about 5 Sv near $\gamma^n \approx 28.2\ kg\ m^{-3}$*. The corresponding peak values of the separate regional curves are approximately 4.0 Sv in the Pacific, 2.3 Sv in the Atlantic, and 1.3 Sv in the Indian Ocean. This regional partition supports the Southern Ocean as the leading regional gateway for upward transformation of bottom-water influence in the diagnosed fields. These regional maxima characterize separate density-dependent curves; contributions to transport across a common surface must be compared at the same density."*

At the same time, we agree that these checks do not demonstrate complete product independence. WOA23 provides an independent hydrographic comparison, but it does not provide an alternative dynamically consistent velocity field with which the full CART and diapycnal-velocity analysis can be repeated. A complete assessment of reanalysis dependence would therefore require repeating the analysis with one or more additional ocean reanalyses.

We have made this distinction explicit by expanding the corresponding limitation in the Discussion. The revised text now reads:

"Because the present analysis relies on a single ocean reanalysis, regional structures and transport magnitudes remain subject to product-dependent uncertainty. Local neutral-density inversions are rare in the three-dimensional GLORYS12 field, and the γ^n*=28.1 kg m*$^{-3}$ *surface used for the principal mapped diagnostics is effectively single-valued (Supplementary Text S1 and Fig. S4b). The comparison with the observationally based World Ocean Atlas 2023 (WOA23) climatology shows broadly similar basin-scale stratification, but the* γ^n *= 28.2 kg m*$^{-3}$ *contour has a more southerly extent in the WOA23 zonal-mean sections of the Atlantic, Pacific, and Indian Oceans (Supplementary Figs. S3 and S8). Differences in bottom density near this label (Supplementary Fig. S9) can alter the occurrence and available area of a fixed density surface. The inversion and uniqueness checks establish the local geometry used for the diagnostics, while the hydrographic comparison identifies differences in the represented dense-water structure. The regional transport magnitudes and their density dependence are therefore interpreted within the GLORYS12 framework. Within this framework, the Southern Ocean's leading regional contribution is evident across a range of density surfaces (Supplementary Fig. S5) and is supported by the concentration and ventilation-thickness patterns (Figs. 3 and 4). These complementary diagnostics support the regional interpretation without establishing that the exact transport magnitudes are independent of the hydrographic product."*

These checks document the near-uniqueness of the mapped GLORYS12 density surface, broad hydrographic agreement together with differences in dense-water extent, and the regional transport partition within GLORYS12. The revised text therefore distinguishes the support for the regional interpretation within this framework from uncertainty in exact regional transports and dense-surface geometry.

2. The methods section is too brief and makes understanding and evaluating the results almost impossible, particularly for readers unfamiliar with the Constituent-oriented Age and Residence Time Theory. More details should be provided, and major quantities presented in figures should be introduced to readers in a more accessible way.

Response: Thank you for this important comment. We agree that the Methods section in the original manuscript was too condensed, particularly for readers who are not familiar with the Constituent-oriented Age and Residence time Theory (CART), and that several diagnostics used later in the figures were not introduced sufficiently clearly before the Results.

We have therefore substantially expanded and reorganized the Methods section. The revised Methods now provide a more complete and structured description of the principal diagnostics used in the study: Sect. 2.1 introduces the CART concentration and water-age formulation, Sect. 2.2 defines ventilation thickness, Sect. 2.3 describes the diapycnal-velocity diagnostic, and Sect. 2.4 defines concentration-weighted diapycnal transport. This organization allows the principal quantities shown in Figs. 2–6 to be defined before their results are presented.

In Sect. 2.1, we have expanded the theoretical description of CART from the underlying age-distribution concentration. Specifically, C and Γ are now explicitly defined as the zeroth and first moments of the local age distribution, and the water age $A = \Gamma/C$ is identified as the concentration-weighted mean age of the bottom-water-origin tracer. The revised text now reads:

> *"Following the CART formulation of Deleersnijder et al. (2001), the age-distribution concentration of the bottom-water-origin tracer at location* x *and time* t *is represented by* $c(x,t,\tau)$*, where* τ *denotes tracer age. The bottom-water concentration* C *and age concentration* Γ *are respectively the zeroth and first moments of this age distribution,*
>
> $$C(x, t) = \int_0^{\infty} c(x, t, \tau)\, d\tau \qquad (1a)$$
>
> $$\Gamma(x, t) = \int_0^{\infty} \tau\, c(x, t, \tau)\, d\tau \qquad (1b)$$
>
> *The water age is then defined as*
>
> $$A(x, t) = \frac{\Gamma(x, t)}{C(x, t)} = \frac{\int_0^{\infty} \tau\, c(x, t, \tau)\, d\tau}{\int_0^{\infty} c(x, t, \tau)\, d\tau} \qquad (2)$$

and therefore represents the concentration-weighted mean age of the bottom-water-origin tracer present at that location and time. It is used here to characterize the renewal timescale of bottom-water influence in Sect. 3.3."

We have also clarified the numerical implementation of the CART equations, including the tracer diffusivity, initial conditions, source-layer treatment, and the meaning of the 100-year integration. The diffusivity used in the tracer equations is now explicitly described as a vertical turbulent diffusivity diagnosed offline using KPP, with no explicit horizontal diffusivity included. The initial and source-layer conditions are also stated explicitly. The revised text now reads:

"To represent bottom-water-origin ventilation, the concentration is initialized as

$$C(x,0) = \begin{cases} 1, x \in \Omega_b \\ 0, x \in \Omega_i \end{cases} \quad (4)$$

where Ω_b denotes the model bottom layer and Ω_i denotes the ocean interior. The initial age concentration is set to $\Gamma(x,0) = 0$ throughout the domain. During the integration, the model bottom layer is continuously restored to C=1:

$$C(x,t) = 1, \quad x \in \Omega_b, \quad t > 0, \quad (5)$$

This prescription provides a continuous source of newly introduced bottom-water tracer, with zero age assigned at the source layer.

Using these initial and source-layer conditions, the CART equations are integrated continuously for 100 years under the monthly climatological forcing derived from GLORYS12. Here, the 100-year period denotes the model integration time under the climatological forcing rather than 100 calendar years of transient ocean evolution. The diagnosed ages measure elapsed time for the tagged component under the repeated climatological annual cycle. Water age is diagnosed as $A = \Gamma / C$ only where $C > 0$. At locations where $C = 0$, or where the resulting age value is numerically invalid, A is assigned NaN and excluded from subsequent diagnostics."

This clarification also makes explicit that the diagnosed water ages characterize renewal under the climatological forcing rather than literal calendar ages in the time-varying ocean.

To make the relationship among the diagnostics explicit, we also revised the end of Sect. 2.1. The revised text now reads:

"The CART calculation therefore provides the concentration and water-age fields used to diagnose the spatial imprint and renewal timescale of bottom-water influence. From the concentration field, we derive the ventilation-thickness diagnostic described in Sect. 2.2. We then diagnose diapycnal

velocity in Sect. 2.3 and combine it with the CART concentration field in Sect. 2.4 to quantify concentration-weighted diapycnal transport."

In addition, the two principal derived diagnostics that were previously introduced too late in the manuscript are now given dedicated Methods subsections. Sect. 2.2 formally defines ventilation thickness and explains its physical interpretation, while Sect. 2.4 defines the concentration-weighted diapycnal transport and explains how it links the CART tracer field with the independently diagnosed diapycnal velocity. The diapycnal-velocity subsection has correspondingly been reorganized as Sect. 2.3 so that its physical motivation, moving-density-surface formulation, and relationship to the tracer-based diagnostics are introduced in a more coherent sequence.

We have also made the principal diagnostics more accessible when they first appear in the Introduction. The revised text now reads:

"Here we combine the high-resolution (1/12°) GLORYS12 global ocean reanalysis with Constituent-oriented Age and Residence time Theory (CART) to diagnose bottom-water return using four complementary metrics: bottom-water concentration to identify the spatial imprint of bottom-water influence, ventilation thickness to characterize its vertically integrated expression, concentration-weighted diapycnal transport to quantify the cross-isopycnal transport associated with that influence, and water age to characterize renewal timescales."

Together, these revisions provide a more complete introduction to CART, clarify the numerical implementation of the tracer experiment, define the major quantities before they are used in the analysis, and establish a clearer methodological framework for interpreting the results.

3. A few figures and their descriptions did not match and should be addressed during revision. For instance, features described in the text (lines 240-250) did not appear in Figure 3, unless I misunderstood them. Also, Figure 1 is difficult to understand. Isopycnal upwelling was marked in the initial state panel but was not mentioned in the caption. Is it important?

Response: Thank you for this helpful comment. We agree that the relationship between several figure features and their descriptions was not sufficiently clear in the original manuscript. We have carefully re-examined the relevant figures and revised both the description of Fig. 3 and the conceptual schematic in Fig. 1.

Regarding Fig. 3, the original text combined features directly visible in the ventilation-thickness maps with a physical interpretation based on comparison with the independently diagnosed diapycnal-velocity field in Fig. 2. This could give the impression that the topographic hotspots and strong diapycnal-exchange regions discussed in the text were explicitly shown or marked in Fig. 3. Figure 3 itself shows only the spatial distribution and temporal evolution of ventilation thickness. We have therefore revised the corresponding Results text so that the patterns directly shown in

Fig. 3 are described first, and the comparison with Fig. 2 is identified explicitly as a cross-diagnostic interpretation.

The revised text now reads:

> *"During the initial stages of the CART integration (integration years 1 and 10; Fig. 3a, b), ventilation thickness remains relatively weak and spatially patchy, with the more prominent signals occurring in the Southern Ocean and in a limited number of boundary-associated regions. Comparison with the independently diagnosed diapycnal velocity in Fig. 2 shows that several of these enhanced regions occur near areas of strong cross-isopycnal exchange, particularly within the Southern Ocean. This spatial correspondence suggests that localized diapycnal transformation contributes to organizing the early spread of bottom-water influence (Baker et al., 2023; Ferrari, 2014; Ferrari et al., 2016; Ledwell et al., 2000; Wynne-Cattanach et al., 2024).*
>
> *By integration years 50 and 100 (Fig. 3c, d), the ventilated footprint expands across all major basins while remaining strongly heterogeneous. The Southern Ocean exhibits the broadest and most coherent ventilation-thickness signals, including enhanced influence near Drake Passage and the Weddell Sea, while additional maxima occur in the tropical-subtropical Pacific, along parts of the Atlantic western boundary system, and in the southern Indian Ocean. Because the global bottom layer is tagged uniformly in the CART experiment, the enhanced Weddell Sea signal reflects strong bottom-water influence in this sector but cannot by itself distinguish contributions from local formation and recirculation, export from the marginal sea, or subsequent cross-isopycnal transformation. Overall, Fig. 3 documents the progressive expansion of bottom-water influence from a relatively patchy early footprint to a broader but still spatially uneven global pattern."*

We have also clarified the temporal labels in Fig. 3 so that the four panels refer explicitly to CART integration years rather than calendar years. The revised caption now reads:

> *"Figure 3 Global distribution of bottom-water ventilation thickness (m) at CART integration years (a) 1, (b) 10, (c) 50, and (d) 100. These years refer to common CART integration times under the repeated climatological forcing, rather than the locally diagnosed quasi-equilibrium sampling times defined in Sect. 2.1. Ventilation thickness represents the vertically integrated bottom-water tracer influence above the continuously restored bottom source layer, which is excluded from the integral."*

Regarding Fig. 1, we agree that the original schematic was difficult to interpret. In particular, the label "Isopycnal upwelling" was imprecise and did not clearly distinguish motion across density surfaces from spreading along them. The process we intended to represent was broader redistribution of the bottom-water signal along density surfaces, whereas the upward transformation across density surfaces is represented by diapycnal upwelling. We have therefore substantially revised the schematic to distinguish these processes explicitly.

The revised Fig. 1 now shows spatially localized zones of bottom-boundary-layer mixing and topographically enhanced internal-wave breaking that generate concentrated diapycnal upwelling, together with broader along-isopycnal spreading of bottom-water signals. The mid-term panel shows bottom-water signals preferentially rising through localized transformation hotspots, and the final panel has been relabeled as a late-integration state to represent the pathway-dependent development of the ventilation-age structure.

The revised Fig. 1 and its caption are shown below:

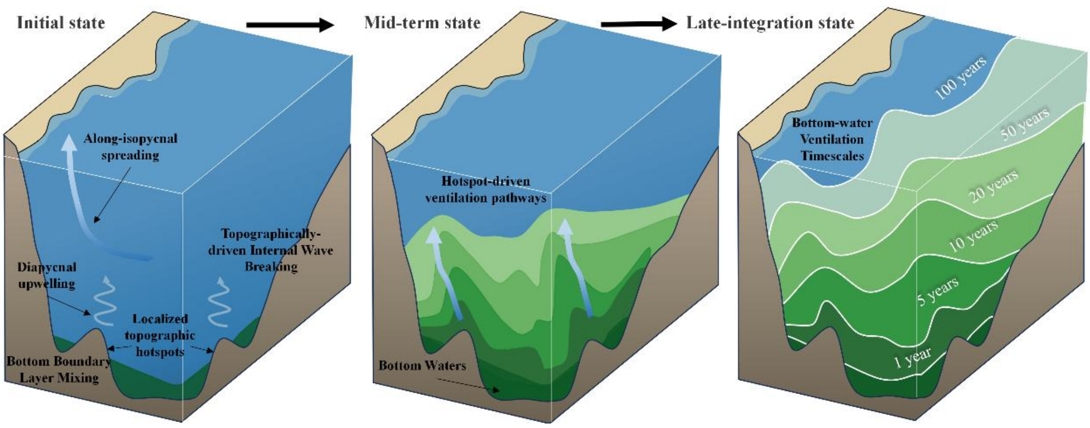

"Figure 1 Conceptual schematic of global bottom-water upward ventilation. In the initial state, dense bottom waters occupy abyssal layers. Bottom-boundary-layer mixing and topographically enhanced internal-wave breaking generate spatially localized zones of diapycnal upwelling, while bottom-water signals may spread more broadly along density surfaces. In the mid-term state, bottom-water signals preferentially rise through these localized hotspots and form spatially heterogeneous ventilation pathways into the ocean interior. In the late-integration state, bottom-water influence extends through the ocean interior, with ventilation timescales increasing away from source and transformation regions. The schematic emphasizes the coupled roles of localized diapycnal transformation, broader along-isopycnal spreading, and pathway-dependent renewal in organizing abyssal bottom-water return."

We also revised the corresponding Introduction text to make the intended connection between the conceptual schematic and the diagnosed spatial heterogeneity explicit. The revised text now reads:

"These processes imply that abyssal bottom-water return is organized around spatially localized transformation hotspots and preferential

dynamical pathways rather than a single diffuse background upwelling field, as summarized schematically in Fig. 1."

4. The presentation of the paper needs improvement. For instance, important concepts, like ventilation thickness, should be explained the first time they appear. In the current version, they have been used many times before being defined. This makes the paper extremely difficult to read and understand.

Response: Thank you for this important comment. We agree that several key diagnostics were introduced too late in the original manuscript. In particular, ventilation thickness was first formally defined in the Results, even though it had already been used earlier in the manuscript, and the concentration-weighted diapycnal transport was likewise introduced together with its results rather than in the Methods. This organization made the diagnostic framework unnecessarily difficult to follow.

We have therefore reorganized the Methods so that the principal quantities used in the Results are defined before they are analyzed. The revised Methods are now organized as Sect. 2.1 for the CART concentration and water-age diagnostics, Sect. 2.2 for ventilation thickness, Sect. 2.3 for diapycnal velocity, and Sect. 2.4 for concentration-weighted diapycnal transport.

To provide an intuitive description when these quantities first appear in the main text, we also revised the corresponding sentence in the Introduction. The revised text now reads:

"Here we combine the high-resolution (1/12°) GLORYS12 global ocean reanalysis with Constituent-oriented Age and Residence time Theory (CART) to diagnose bottom-water return using four complementary metrics: bottom-water concentration to identify the spatial imprint of bottom-water influence, ventilation thickness to characterize its vertically integrated expression, concentration-weighted diapycnal transport to quantify the cross-isopycnal transport associated with that influence, and water age to characterize renewal timescales."

We moved the definition of ventilation thickness from the Results to a new Methods subsection. The new Sect. 2.2 now reads:

*"**2.2 Ventilation thickness***

To quantify the vertically integrated influence of bottom-water-origin tracer at each horizontal location, we define the ventilation thickness as

$$T_{vent}(x, y, t) = \int_{z_b}^{z_s} C(x, y, z, t)\, dz, \qquad (6)$$

where z_b denotes the upper boundary of the continuously restored bottom source layer and z_s denote the local surface level. The restored bottom source layer itself is excluded from the vertical integral so that its prescribed concentration of C=1 does not contribute a fixed background *inventory associated with the local thickness of the bottom grid cell. Because C is dimensionless and represents the local fraction of bottom-water-origin tracer,* T_{vent} *has units of meters. It measures the equivalent column-integrated imprint of bottom-water influence, distinct from the physical depth of the water column. Larger values therefore indicate either stronger bottom-water concentration, a greater vertical extent of bottom-water influence, or a combination of both. This diagnostic complements the local concentration field by summarizing the vertical extent and strength of bottom-water influence in a single two-dimensional quantity."*

Correspondingly, after moving the formal definition of ventilation thickness to the Methods, we streamlined the Results so that the text now moves directly from the diagnostic framework to its physical interpretation. The revised transition now reads:

"As a column-integrated diagnostic, ventilation thickness provides a compact view of where abyssal return first emerges, how broadly it expands, and where it is expressed most strongly through the full water column. Its evolution at CART integration years 1, 10, 50, and 100 is shown in Fig. 3."

The original diapycnal-velocity subsection has consequently been renumbered as Sect. 2.3, and its opening has been revised to connect the tracer-based and dynamical diagnostics. The revised opening now reads:

"Bottom-water return requires not only the spreading of bottom-water-origin signals through the ocean interior, but also cross-isopycnal transformation that transfers these waters into lighter density classes and ultimately reconnects them with the upper ocean (Ferrari, 2014; Lumpkin and Speer, 2007; Marshall and Speer, 2012; Talley, 2013). Such diapycnal exchange is strongly heterogeneous in space, with enhanced mixing occurring preferentially near rough topography, ocean boundaries, and dynamically active regions of the Southern Ocean (Cimoli et al., 2023; Ledwell et al., 2000; Ruan and Ferrari, 2021; Wynne-Cattanach et al., 2024). To provide the dynamical counterpart to the tracer-based diagnostics introduced above, we therefore diagnose diapycnal velocity, which represents the rate of water motion across moving density surfaces and identifies where cross-density exchange can support bottom-water transformation and upward return (Bennett, 1986; Ferrari et al., 2016; Marshall et al., 1999)."

We also moved the definition of concentration-weighted diapycnal transport from the Results to a new Sect. 2.4. The new subsection now reads:

*"**2.4 Concentration-weighted diapycnal transport***

Diapycnal velocity identifies where cross-density exchange occurs, but it does not distinguish whether that exchange acts on water carrying a substantial bottom-water-origin signal. To connect the dynamical field with the CART concentration field, we therefore diagnose a concentration-

weighted analogue of the water-mass transformation rate, which is conventionally defined from the integral of diapycnal velocity across density surfaces (Cimoli et al., 2023; Ferrari et al., 2016).

The concentration-weighted diapycnal transport is defined as

$$\Phi_C(\gamma^n) = \int_{A(\gamma^n)} C\omega_d \, dA, \quad (9)$$

where $A(\gamma^n)$ *denotes the isopycnal surface over which the area integral is evaluated,* ω_d *is the signed scalar diapycnal velocity normal to the neutral-density surface defined in Sect. 2.3,* n_ρ *is the unit normal vector to the density surface, and* C *is the bottom-water concentration sampled at the local diagnostic times defined in Sect. 2.1.*

Physically, Φ_C *measures the component of diapycnal transport associated with bottom-water influence. It therefore differs from a conventional water-mass transformation diagnostic by weighting the diapycnal exchange with the fraction of bottom-water origin. Regions with strong diapycnal motion but weak bottom-water concentration contribute little to* Φ_C*, whereas regions where upward diapycnal motion coincides with high bottom-water concentration make the largest contribution to the transformation of bottom-water influence. Here positive values indicate transport toward denser classes (downwelling), whereas negative values indicate transport toward lighter classes (upwelling). Interpreted together with the concentration fields, this diagnostic identifies where upward transformation of bottom-water influence is strongest."*

Similarly, after moving the definition of concentration-weighted diapycnal transport to Sect. 2.4, we revised the corresponding Results transition to avoid repeating methodological material. The revised text now reads:

"To connect the concentration pathways identified above with cross-isopycnal transformation, we next examine the concentration-weighted diapycnal transport defined in Sect. 2.4."

Furthermore, we also revised the closing paragraph of Sect. 2.1 to clarify how the CART-derived fields are connected to the additional diagnostics introduced in the subsequent Methods subsections. The revised text now reads:

"The CART calculation therefore provides the concentration and water-age fields used to diagnose the spatial imprint and renewal timescale of bottom-water influence. From the concentration field, we derive the ventilation-thickness diagnostic described in Sect. 2.2. We then diagnose diapycnal velocity in Sect. 2.3 and combine it with the CART concentration field in Sect. 2.4 to quantify concentration-weighted diapycnal transport."

References cited in this response

Artana, C., Ferrari, R., Bricaud, C., Lellouche, J.-M., Garric, G., Sennéchael, N., Lee, J.-H., Park, Y.-H., and Provost, C.: Twenty-five years of Mercator ocean reanalysis GLORYS12 at Drake Passage: Velocity assessment and total volume transport, Adv. Space Res., 68, 447–466, https://doi.org/10.1016/j.asr.2019.11.033, 2021.

Baker, L. E., Mashayek, A., and Naveira Garabato, A. C.: Boundary Upwelling of Antarctic Bottom Water by Topographic Turbulence, AGU Adv., 4, e2022AV000858, https://doi.org/10.1029/2022AV000858, 2023.

Bennett, S. L.: The Relationship between Vertical, Diapycnal, and Isopycnal Velocity and Mixing in the Ocean General Circulation, J. Phys. Oceanogr., 16, 167–174, https://doi.org/10.1175/1520-0485(1986)016<0167:TRBVDA>2.0.CO;2, 1986.

Cimoli, L., Mashayek, A., Johnson, H. L., Marshall, D. P., Naveira Garabato, A. C., Whalen, C. B., Vic, C., De Lavergne, C., Alford, M. H., MacKinnon, J. A., and Talley, L. D.: Significance of Diapycnal Mixing Within the Atlantic Meridional Overturning Circulation, AGU Adv., 4, e2022AV000800, https://doi.org/10.1029/2022AV000800, 2023.

Deleersnijder, E., Campin, J.-M., and Delhez, E. J. M.: The concept of age in marine modelling I. Theory and preliminary model results, J. Mar. Syst., 28, 229–267, https://doi.org/10.1016/S0924-7963(01)00026-4, 2001.

Du Pontavice, H., Chen, Z., and Saba, V. S.: A high-resolution ocean bottom temperature product for the northeast U.S. continental shelf marine ecosystem, Prog. Oceanogr., 210, 102948, https://doi.org/10.1016/j.pocean.2022.102948, 2023.

Ferrari, R.: What goes down must come up, Nature, 513, 179–180, https://doi.org/10.1038/513179a, 2014.

Ferrari, R., Mashayek, A., McDougall, T. J., Nikurashin, M., and Campin, J.-M.: Turning Ocean Mixing Upside Down, J. Phys. Oceanogr., 46, 2239–2261, https://doi.org/10.1175/JPO-D-15-0244.1, 2016.

Jean-Michel, L., Eric, G., Romain, B.-B., Gilles, G., Angélique, M., Marie, D., Clément, B., Mathieu, H., Olivier, L. G., Charly, R., Tony, C., Charles-Emmanuel, T., Florent, G., Giovanni, R., Mounir, B., Yann, D., and Pierre-Yves, L. T.: The Copernicus Global 1/12° Oceanic and Sea Ice GLORYS12 Reanalysis, Front. Earth Sci., 9, 698876, https://doi.org/10.3389/feart.2021.698876, 2021.

Ledwell, J. R., Montgomery, E. T., Polzin, K. L., St. Laurent, L. C., Schmitt, R. W., and Toole, J. M.: Evidence for enhanced mixing over rough topography in the abyssal ocean, Nature, 403, 179–182, https://doi.org/10.1038/35003164, 2000.

Lellouche, J.-M., Greiner, E., Le Galloudec, O., Garric, G., Regnier, C., Drevillon, M., Benkiran, M., Testut, C.-E., Bourdalle-Badie, R., Gasparin, F., Hernandez, O., Levier, B., Drillet, Y., Remy, E., and Le Traon, P.-Y.: Recent updates to the Copernicus Marine Service global ocean monitoring and forecasting real-time 1/12° high-resolution system, Ocean Sci., 14, 1093–1126, https://doi.org/10.5194/os-14-1093-2018, 2018.

Lumpkin, R. and Speer, K.: Global Ocean Meridional Overturning, J. Phys. Oceanogr., 37, 2550–2562, https://doi.org/10.1175/JPO3130.1, 2007.

Marshall, J. and Speer, K.: Closure of the meridional overturning circulation through Southern Ocean upwelling, Nat. Geosci., 5, 171–180, https://doi.org/10.1038/ngeo1391, 2012.

Marshall, J., Jamous, D., and Nilsson, J.: Reconciling thermodynamic and dynamic methods of computation of water-mass transformation rates, Deep-Sea Res. Pt. I, 46, 545–572, https://doi.org/10.1016/S0967-0637(98)00082-X, 1999.

Ruan, X. and Ferrari, R.: Diagnosing Diapycnal Mixing from Passive Tracers, J. Phys. Oceanogr., 51, 757–767, https://doi.org/10.1175/JPO-D-20-0194.1, 2021.

Talley, L.: Closure of the Global Overturning Circulation Through the Indian, Pacific, and Southern Oceans: Schematics and Transports, Oceanography, 26, 80–97, https://doi.org/10.5670/oceanog.2013.07, 2013.

Verezemskaya, P., Barnier, B., Gulev, S. K., Gladyshev, S., Molines, J., Gladyshev, V., Lellouche, J., and Gavrikov, A.: Assessing Eddying (1/12°) Ocean Reanalysis GLORYS12 Using the 14-yr Instrumental Record From 59.5°N Section in the Atlantic, J. Geophys. Res.-Oceans, 126, e2020JC016317, https://doi.org/10.1029/2020JC016317, 2021.

Wynne-Cattanach, B. L., Couto, N., Drake, H. F., Ferrari, R., Le Boyer, A., Mercier, H., Messias, M.-J., Ruan, X., Spingys, C. P., Van Haren, H., Voet, G., Polzin, K., Naveira Garabato, A. C., and Alford, M. H.: Observations of diapycnal upwelling within a sloping submarine canyon, Nature, 630, 884–890, https://doi.org/10.1038/s41586-024-07411-2, 2024.